



Direct observation of Lévy flights of holes in bulk n -doped InP

Serge Luryi, Oleg Semyonov, Arsen Subashiev, and Zhichao Chen

State University of New York at Stony Brook, Stony Brook, New York, 11794-2350, USA

(Received 21 May 2012; published 19 November 2012)

We study the photoluminescence spectra excited at an edge side of n -InP slabs and observed from the broadside. In a moderately doped sample the intensity drops off as a power-law function of the distance from the excitation—up to several millimeters—with no change in the spectral shape. The hole distribution is described by a stationary Lévy-flight process over more than two orders of magnitude in both the distance and hole concentration. For heavily doped samples, the power law is truncated by free-carrier absorption. Our experiments are nearly perfectly described by the Biberman-Holstein transport equation with parameters found from independent optical experiments.

DOI: [10.1103/PhysRevB.86.201201](https://doi.org/10.1103/PhysRevB.86.201201)

PACS number(s): 78.55.Cr, 05.40.Fb, 78.30.Fs, 78.60.Lc

The transport of minority carriers produced by optical excitation in semiconductors is usually well described by a diffusion equation. Then the concentration decay from the excitation area can be characterized by a diffusion length $l = \sqrt{D\tau}$, with D being the diffusivity of carriers and τ their lifetime. The diffusion process can be viewed as the result of a random walk in which every step x_i has the same probability density $\mathcal{P}(x_i)$. In moderately doped direct-gap semiconductors, the transport of minority carriers is modified by a repeated radiative recombination and subsequent reabsorption of emitted photons, a process called “photon recycling.”

The energy relaxation time for nonequilibrium minority carriers, created by reabsorption, is due to electron-phonon interaction and at room temperature it is in the picosecond range.¹ It is much shorter than the radiative recombination time τ_{rad} (mean time before the next photon is emitted), which even in direct semiconductors is at least 10 ns.^{2,3} Therefore, the reemission spectrum of secondary photons coincides with the recombination spectrum of minority carriers in quasiequilibrium with the lattice. This means that reemitted photons are statistically independent and the steps x_i can be characterized by a single step distribution function $\mathcal{P}(x)$. Since the photon-assisted transport is mediated by interband photons, the $\mathcal{P}(x)$ is specified through the absorption spectrum of these photons.

If the second moment $\langle x^2 \rangle$ of $\mathcal{P}(x)$ is finite, one can define a photon-assisted (recycling) contribution to the diffusion coefficient, $D_{\text{ph}} \propto \langle x^2 \rangle / \langle \tau \rangle$, where $\langle \tau \rangle = \tau_{\text{rad}}$ is the mean time between steps. The recycling contribution may lead to a substantial enhancement of D and l , but the diffusion description would still be applicable.

If, however, the step distribution is heavy tailed, asymptotically satisfying a power law

$$\mathcal{P}(x) \sim 1/x^{\gamma+1}, \quad (1)$$

with $0 \leq \gamma \leq 1$, then the conventionally defined diffusivity diverges and the random walk is governed by rare but large steps.⁴ Such a transport, called the Lévy flight, features an anomalously large spread in space and a “superdiffusive” temporal evolution.⁵⁻⁷

Superdiffusive transport of light has been known in the context of radiation trapping in propagation through media with narrow absorption lines. This phenomenon occurs in

different systems, ranging from stars^{8,9} to dense atomic vapors,¹⁰ such as gas lasers, discharges, and hot plasmas. It has been studied for many decades, starting from the theoretical papers by Biberman¹¹ and Holstein.¹² Recently, Lévy flights of photons were directly observed in engineered optical materials¹³ and in hot vapors.¹⁴ Direct-gap semiconductors represent a new and exciting “lab” system for studying the Lévy flight of photons and/or minority carriers.^{15,16}

We have investigated¹⁵ the step distribution $\mathcal{P}(x)$ for the photon-assisted transport of holes in moderately doped n -InP and found that it asymptotically obeys the power law (1) with $\gamma = 0.7$. For heavier doping, the power law is truncated by free-carrier absorption,

$$\mathcal{P}(x) \sim (1/x^{\gamma+1})e^{-\alpha_{\text{fc}}x}, \quad (2)$$

where α_{fc} (cm^{-1}) $\approx 1.3 \times 10^{-18} N_d$ is the free-carrier absorption coefficient in InP.^{3,17}

The resultant random walk is limited by the loss of carriers in nonradiative recombination (of rate τ_{nr}^{-1}). The relative rates of recombination are characterized by the radiative efficiency $\eta = \tau_{\text{nr}} / (\tau_{\text{nr}} + \tau_{\text{rad}})$ and the typical number of steps by the recycling factor $\Phi = \eta / (1 - \eta)$. Due to its high radiative efficiency (with Φ reaching 10^2 for moderately doped samples), the n -doped InP is ideally suited for studying the Lévy flight of holes.^{3,15-17} The key parameters (γ and Φ) can be controlled by varying the doping N_d and the temperature. The truncation length α_{fc}^{-1} can also be controlled by varying N_d .

In earlier photoluminescence experiments with n -InP we found an indirect evidence of the Lévy flight of holes by analyzing the ratio of transmitted and reflected luminescence spectra across a thin flat wafer.¹⁵

A very different geometry is used in this work: The luminescence is excited at an edge side of the wafer and observed from the broadside (Fig. 1). The luminescence intensity measured as a function of the distance x from the edge is directly proportional to the hole distribution $p(x)$ in the sample. In a moderately doped sample, we observe a power-law distribution, providing an unambiguous manifestation of the Lévy flight of holes. In samples of heavier doping, $p(x)$ evolves toward a distribution characteristic of truncated Lévy flight.

We have studied three n -InP samples¹⁸ of thickness $d = 350 \mu\text{m}$ and doping $N_d = 0.3, 2, \text{ and } 6 \times 10^{18} \text{ cm}^{-3}$ (samples I, II, and III, respectively). A 808-nm laser beam was focused

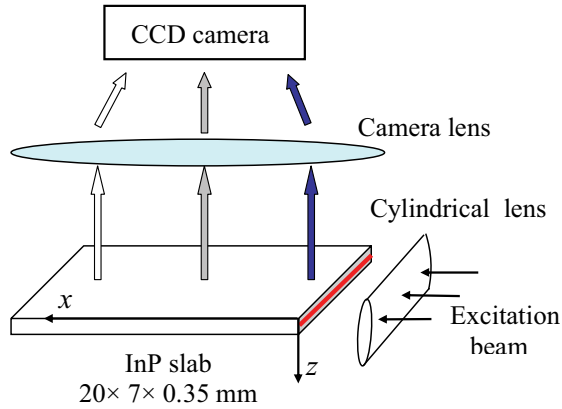


FIG. 1. (Color online) Geometry of our photoluminescence experiment. To avoid scattering by the edges, the laser beam is focused on a narrow strip $z_0 \pm \delta z$ in the 7-mm side of the sample, where $\delta z \approx 50 \mu\text{m}$ and $z_0 \approx 100 \mu\text{m}$, counting from the top surface.

(see Fig. 1) on the 7-mm edge side of the sample using a cylindrical lens. The stationary excitation flux was uniform along the edge. Excitation photon energy $E = 1.53 \text{ eV}$ (above the interband absorption edge at $E_g \approx 1.35 \text{ eV}$) ensured the initial hole generation in a thin (submicron) layer near the surface. Luminescence emitted from the broadside was captured by a lens to project the image on a CCD camera. A razor blade was installed near the excitation edge to obscure the luminescence emitted in the direction of the camera from the edge surface itself.

We have also measured the luminescence spectra at different distances x from the excitation. These normalized spectra are shown in Fig. 2 for sample I. In the range of x from 0.5 to 3 mm, the spectra remain essentially the same and in agreement

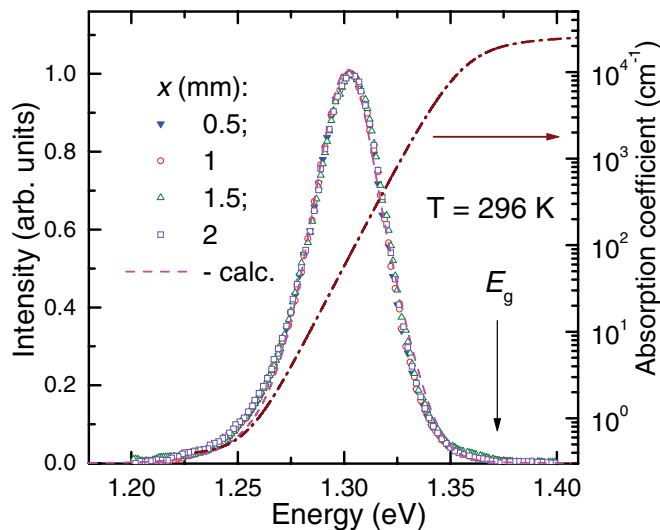


FIG. 2. (Color online) Luminescence spectra observed from the top side of sample I at varying distances from the edge (dots). The dashed line shows the calculated spectra assuming an intrinsic van Roosbroek–Shockley emission spectrum, modified by reabsorption of radiation in the sample. Also shown is the absorption spectrum $\alpha(E)$ exhibiting an Urbach tail of α_i below E_g . The Urbach-tail dependence is masked by the free-carrier absorption only for $E < 1.26 \text{ eV}$.

with the calculated spectrum (dashed line) for a near-uniform hole distribution $p(z) = p(x_0, z) \approx \text{const}$, as expected for any fixed $x_0 \geq d$ (see below).

The absorption spectrum $\alpha(E)$ of sample I is shown in Fig. 2 by a dashed-dotted line. It exhibits an exponential Urbach behavior, extending down to $\alpha \approx 0.5 \text{ cm}^{-1}$. At lower E , the Urbach tail, characteristic of interband absorption α_i , is masked by the free-carrier absorption, $\alpha(E) = \alpha_i(E) + \alpha_{fc}$. Light scattering is negligible in crystalline InP and at long wavelengths the transparency of our samples is limited by α_{fc} . At high E , the Urbach exponent saturates at $E > E_g$. With the higher doping, the absorption edge is shifted to higher energies due to the Moss-Burstein effect. It is notable that the observed luminescence spectrum lies fully in the Urbach-tail region of the absorption spectrum—in contrast with the intrinsic emission spectrum described by the quasiequilibrium van Roosbroek–Shockley¹⁹ relation (VRS),

$$S_{\text{VRS}}(E) \sim \alpha_i E^3 e^{-E/kT}, \quad (3)$$

which has a maximum above E_g .

The luminescence intensity distributions $I(x)$ were obtained by scanning the CCD image along a line parallel to x . To reduce random fluctuations, the distributions were averaged over 20 scans. Additionally, the CCD camera was shifted both in the y and x directions, with the corresponding scans averaged again to reduce irregularities in the response of different pixels. The observed $I(x)$ was strictly proportional to the excitation laser power and hence to the hole concentration $p(x)$. To stay within the linear-response range of CCD over the entire range of x , we first used a neutral filter to reduce $I(x)$ near the excitation edge and then the razor blade was shifted along x to obscure the brightest parts of the slab just near the edge. Subsequently, the filter was removed to get a measurable signal far from the edge. The residual dark noise of the camera was subtracted. The resulting distributions for all three samples are presented in Fig. 3.

For sample I at distances $x > 0.5 \text{ mm}$, a power law $I(x) \sim 1/x^{1+\gamma}$ is clearly observed. This is most easily seen on the log-log scale in the inset of Fig. 3. The best fit for $\gamma = 0.7 \pm 0.1$ agrees with the index γ obtained earlier¹⁵ for $\mathcal{P}(x)$. The power law is in clear contrast to an exponential decay $I(x) \sim \exp(-x/l)$ expected for a (photon-assisted) diffusive spread of holes, even accounting for any enhancement of the diffusion length l by recycling (data fitting by a diffusive curve with $l = 210 \mu\text{m}$ is shown in Fig. 3 by the dashed line).

For samples II and III with higher doping, the heavy tails are also clearly seen. However, the power-law distribution is truncated at large distances. This effect correlates with the increasing $\alpha_{fc}(N_d)$.

The nature of the emission spectra is discussed in detail in the review.¹⁶ Owing to the rapid energy relaxation of holes, the room-temperature intrinsic emission spectrum in n -InP is well described by Eq. (3). The observed spectrum $S(E)$ is strongly redshifted (filtered) by reabsorption on its way in the sample to the surface, $S(E) = S_{\text{VRS}}(E)F(E)$, where $F(E)$ is the spectral filtering function $F(E) = F_1(E)T(E)$, which depends on the hole distribution $p(z)$ across the wafer and is affected by reflections from the sample surfaces. The one-pass

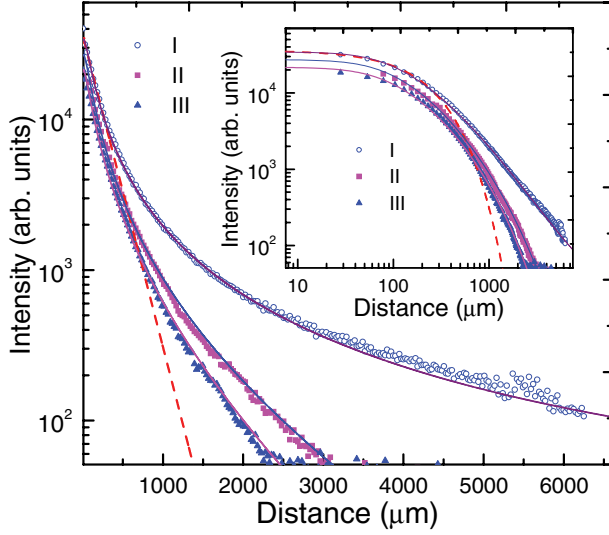


FIG. 3. (Color online) Distribution of the luminescence intensity $I(x)$ and hole concentration $p(x) \propto I(x)$ for three differently doped samples (dots). The results of calculations using optical parameters of the samples are shown by solid lines. For comparison, an exponential distribution with enlarged diffusion length $l = 210 \mu\text{m}$ is also shown (by a dashed line). For the low-doped sample I, the distribution is a power law, with the index γ readily obtained from the slope of the log-log scaled graph in the inset. For samples II and III with higher N_d , the distribution is truncated by free-carrier absorption.

filtering function $F_1(E)$ is given by^{15,16}

$$F_1(E) = \int_0^d p(z) \exp[-\alpha(E)z] dz. \quad (4)$$

The factor $T(E) = \{1 - R \exp[-\alpha(E)d]\}^{-1}$ accounts for the multiple surface reflections, $R(E) \approx 0.33$. Note that due to the high index contrast the radiation escape cone is narrow, i.e., the outgoing radiation propagates close to the normal direction to the surface. Multiple reflections are noticeable only in the red wing of the spectrum.

One can expect that for $x > d$ the hole distribution $p(z)$ is uniform across the sample, except for small regions near the surfaces, where it is distorted by surface recombination. This assumption is confirmed by solving the one-dimensional diffusion equation with a recycling term [see Eq. (6) below] for $p(z)$ with uniform generation at a given x . The calculated emission spectrum is fully determined by parameters of the absorption spectrum. Results of the calculations, shown in Fig. 2 by a dashed line, agree with experiment nearly perfectly, without adjustable parameters. The position of the emission line maximum can be calculated analytically by substituting $p(z) = \text{const}$ into Eq. (4). Near the center of the emission line the absorption coefficient is described by a simple exponent, $\alpha = \alpha_0 \exp[(E - E_g)/\Delta]$, with the parameters $\alpha_0 = 1.1 \times 10^4 \text{ cm}^{-1}$, $E_g = 1.354 \text{ eV}$, $\Delta = 9.4 \text{ meV}$, known from optical studies.^{17,20} The emission line peak position E_{max} is then found from the equation $dS(E)/dE = 0$, which gives

$$E_{\text{max}} = E_g - \Delta \ln(\alpha_0 d/s), \quad (5)$$

where s is a nonzero solution of transcendental equation $(kT/\Delta)s = [\exp(s) - 1]$. This gives $E_{\text{max}} = 1.303 \text{ eV}$, in agreement with experiment. The excellent agreement further confirms both the VRS shape (3) of the intrinsic spectrum and the proportionality $p(x) \propto I(x)$.

Next we discuss the hole distribution $p(x)$ along the sample. Since the excitation is restricted to a narrow region near the edge surface, and all surfaces are highly reflective due to a narrow radiation escape cone, this distribution can be found from the one-dimensional Biberman-Holstein stationary transport equation^{8,11,12,16}

$$-D \frac{\partial^2 p(x)}{\partial x^2} + \frac{p(x)}{\tau} = G(x) + \frac{\eta}{\tau} \int_{-\infty}^{\infty} p(x') \mathcal{P}(|x - x'|) dz', \quad (6)$$

where D is the ordinary hole diffusivity and τ^{-1} is the total recombination rate. The last term on the right-hand side accounts for the photon recycling. The reflection from the edge face at $x = 0$ is included by assuming a symmetric distribution $p(x) = p(-x)$ and extending the integration to $-\infty$ (which supplies an image source for every radiative recombination event in the sample). Here $\mathcal{P}(|x - x'|)$ is the probability, averaged over the plane $x = \text{const}$, of a hole to generate another hole at a distance $|x - x'|$ by the emission-reabsorption process (see Ref. 16):

$$\mathcal{P}(|x|) = \frac{1}{2} \int_0^{\infty} \mathcal{N}(E) \alpha_i(E) \text{Ei}(1, \alpha(E)|x|) dE, \quad (7)$$

where $\text{Ei}(1, x) = \int_1^{\infty} dt t^{-1} \exp(-xt)$ is an exponential integral. The integrand in Eq. (7) is a product of probabilities for (i) emission of a photon at energy E , described by a normalized spectral function $\mathcal{N}(E) \propto E^{-1} S_{\text{VRS}}(E)$, (ii) propagation of this photon from a point at distance x to another point at distance x' , described by the factor $\text{Ei}(1, \alpha(E)|x|)$, and (iii) interband absorption of this photon, represented by the factor $\alpha_i(E)$. Hence, neglecting the very small effects of hole displacement in their thermal motion, the function $\mathcal{P}(|x - x'|)$ is the single-step length distribution for holes. The probability $\mathcal{P}(|x|)$ given by Eq. (7) is again fully determined by the absorption spectrum and can be calculated numerically.^{15,16} For all $x \geq 1 \mu\text{m}$, it obeys the power law (2) with an exponential factor allowing for free-carrier absorption. The index of the distribution is fully determined by the Urbach-tail part of the spectrum and is given by $\gamma = 1 - \Delta/kT$.

A solution of Eq. (6) can be obtained by a Fourier transformation. For $G = G_0 \delta(x)$ it is of the form

$$p(x) = \frac{G_0 \tau}{\pi} \int_0^{\infty} \frac{\cos(kx)}{1 + l^2 k^2 - \eta F(k)} dk. \quad (8)$$

Here $l = \sqrt{D\tau}$ is the ordinary hole diffusion length, and $F(k)$ is the Fourier transform of $\mathcal{P}(|x|)$. The effects of recycling are negligible for small η (≤ 0.5) and in this limit one obtains from Eq. (8) the usual exponential decay with the characteristic length l . Another exponent is obtained from (8) if the carrier spread in recycling is neglected. In this limit, $F(k) \rightarrow 1$, we find a “recycling enhanced diffusion length” $\sim l\sqrt{\Phi}$. For $x \gg l$ the distribution $p(x)$ is fully determined by $F(k)$ (and hence in turn by the absorption spectrum). The only additional parameter η has been already evaluated for

each sample—from the time-resolved luminescence kinetics experiments³ and, independently, by analyzing the ratio of transmission-to-reflection luminescence spectra.¹⁵

An alternative to solving Eq. (6) is to do Monte Carlo modeling of the hole distribution using the single-step probability (7).^{15,16} The result coincides with (8) at distances $x < 500 \mu\text{m}$. However, at considerably larger distances of interest to us here, the Monte Carlo approach becomes noisy and therefore less reliable.²¹

Results of the numerical calculations of $p(z)$ using (8) for all samples are shown by the solid lines in Fig. 3, demonstrating an excellent agreement with the experimental data, except for a slight discrepancy for the heaviest doped sample III (see below).

The main features of the distribution are revealed by an analytic approximation that can be derived directly from Eq. (6). At large distances, due to the heavy tail of $\mathcal{P}(|x|)$, one can solve Eq. (6) by sequential iterations—making in all terms of the resultant series the “longest step approximation”⁸ (i.e., choosing one of the steps equal the total distance x). This gives

$$p(x) = \frac{\Phi \mathcal{P}(x)}{[1 + \Phi \mathcal{P}_e(x)]^2}, \quad (9)$$

where $\mathcal{P}_e(x) = \int_x^\infty \mathcal{P}(x') dx'$ is the probability of escape beyond x in one step. Equation (9) provides a good approximation to the exact solution in the entire range of x . It works with or without truncation of the Lévy flight by free-carrier absorption. Similarly to the “stable distribution,”⁴ distribution (9) asymptotically reproduces the one-step probability (enhanced by the recycling factor Φ) and is modified at

smaller distances. Since $\Phi \mathcal{P}_e(x)$ is the escape probability in Φ attempts, condition $\Phi \mathcal{P}_e(x_f) = 1$ gives the distance x_f to the “front” of $p(x)$ —beyond which the holes appear predominantly in one step. The front x_f is clearly seen in the inset of Fig. 3, as the point of maximum curvature on the log-log plots for all samples. The observed $x_f \approx 200 \mu\text{m}$ manifests the large values of Φ in these samples. For $x \ll x_f$, Eq. (9) correctly predicts the short-distance asymptote,¹⁶ $p(x) \sim 1/x^{1-\gamma}$, but the corresponding data are obscured in our experiment by deviations from the one-dimensional geometry.²² For sample III, the effective front distance x_f is somewhat larger than could be expected from earlier experiments.

In conclusion, we have studied the stationary hole distribution $p(x)$ over distances x of several millimeters from initial photoexcitation. We observe a heavy-tailed decline of the luminescence intensity with no change in the spectral shape. For a low-doped sample, we find a power-law distribution $p(x) \sim 1/x^{1+\gamma}$ with $\gamma = 0.7$ precisely accounted for by the Lévy-flight transport of holes mediated by photon recycling.²³ In heavier-doped samples, the power law is truncated by free-carrier absorption, which manifest itself only at distances $x \sim \alpha_{fc}^{-1}$ corresponding to the free-carrier absorption. The anomalous transport should be important in all semiconductor crystals with high radiative efficiency and may have practical implications in optoelectronic devices.¹⁶

This work was supported by the Domestic Nuclear Detection Office, by the Defense Threat Reduction Agency (basic research program), and by the Center for Advanced Sensor Technology at Stony Brook.

¹V. F. Gantmakher and Y. B. Levinson, *Carrier Scattering in Metals and Semiconductors* (Elsevier, Amsterdam, 1987); K. Seeger, *Semiconductor Physics*, 9th ed. (Springer, Berlin, 2004).

²E. F. Schubert, *Light-Emitting Diodes*, 2nd ed. (Cambridge University Press, Cambridge, UK, 2006).

³O. Semyonov, A. V. Subashiev, Z. Chen, and S. Luryi, *J. Appl. Phys.* **108**, 013101 (2010).

⁴P. Lévy, *Theorie de l'Addition des Variables Aleatoires* (Gauthier-Villiers, Paris, 1937).

⁵J.-P. Bouchaud and A. Georges, *Phys. Rep.* **195**, 127 (1990).

⁶*Lévy Flights and Related Topics in Physics*, edited by M. Shlesinger, G. Zaslavsky, and U. Frisch (Springer, New York, 1995).

⁷R. Metzler and J. Klafter, *Phys. Rep.* **339**, 1 (2000).

⁸V. V. Ivanov, *Transfer of Radiation in Spectral Lines*, transl. edited by D. G. Hummer, Natl. Bur. Stand. (US) Specl. Publ. 385 (U.S.G.P.O., Washington, DC, 1973); G. Rybicki and A. Lightman, *Radiation Processes in Astrophysics* (Wiley, New York, 1979).

⁹U. Springmann, *Astron. Astrophys.* **289**, 505 (1994).

¹⁰A. F. Molisch and B. P. Oehry, *Radiation Trapping in Atomic Vapours* (Clarendon Press, Oxford, 1998).

¹¹L. M. Biberman, *Zh. Eksp. Teor. Fiz.* **17**, 416 (1947); **19**, 584 (1949).

¹²T. Holstein, *Phys. Rev.* **72**, 1212 (1947).

¹³P. Barthelemy, J. Bertolotti, and D. S. Wiersma, *Nature (London)* **453**, 495 (2008).

¹⁴N. Mercadier, W. Guerin, M. Chevrollier, and R. Kaiser, *Nat. Phys.* **5**, 602 (2009).

¹⁵O. Semyonov, A. V. Subashiev, Z. Chen, and S. Luryi, *J. Lumin.* **132**, 1935 (2012).

¹⁶S. Luryi and A. V. Subashiev, *Int. J. High Speed Electron. Syst.* **21**(1), 3 (2012).

¹⁷A. Subashiev, O. Semyonov, Z. Chen, and S. Luryi, *Appl. Phys. Lett.* **97**, 181914 (2010).

¹⁸ACROTEC InP wafers from NIKKO Metals (Japan).

¹⁹W. van Roosbroek and W. Shockley, *Phys. Rev.* **94**, 1558 (1954).

²⁰Urbach-tail parameters in the absorption spectrum of n -InP differ from those of semi-insulating InP, where $E_g = 1.343 \text{ eV}$ and $\Delta = 7.1 \text{ meV}$; compare M. Bugajski and W. Lewandowski, *J. Appl. Phys.* **57**, 521 (1985) and M. Beaudoin *et al.*, *Appl. Phys. Lett.* **70**, 3540 (1997).

²¹A. Clauset, C. R. Shalizi, and M. E. J. Newman, *SIAM Rev.* **51**, 661 (2009).

²²The geometry of the photon transport deviates from one dimensional at short distances ($x \sim d/2$), since the excitation beam is focused and nonuniform in z direction. This effect is taken into account empirically by the replacement $x \rightarrow \sqrt{x^2 + z_0^2}$ with $z_0 \approx 60 \mu\text{m}$ as a fitting parameter. This does not affect the results at $x \geq d$.

²³We have observed an enhancement of this effect (γ gets smaller) at lower temperatures (to be published separately).